Recurrent-Neural-Network-Based Adaptive-Backstepping Control for Induction Servomotors

Chih-Min Lin, *Senior Member, IEEE*, and Chun-Fei Hsu, *Member, IEEE*

***Abstract*—This study is concerned with the position control of an induction servomotor using a recurrent-neural-network (RNN)-based adaptive-backstepping control (RNABC) system. The adaptive-backstepping approach offers a choice of design tools for the accommodation of system uncertainties and nonlinearities. The RNABC system is comprised of a backstepping controller and a robust controller. The backstepping controller containing an RNN uncertainty observer is the principal controller, and the robust controller is designed to dispel the effect of approximation error introduced by the uncertainty observer. Since the RNN has superior capabilities compared to the feedforward NN for dynamic system identification, it is utilized as the uncertainty observer. In addition, the Taylor linearization technique is employed to increase the learning ability of the RNN. Meanwhile, the adaptation laws of the adaptive-backstepping approach are derived in the sense of the Lyapunov function, thus, the stability of the system can be guaranteed. Finally, simulation and experimental results verify that the proposed RNABC can achieve favorable tracking performance for the induction-servomotor system, even with regard to parameter variations and input-command frequency variation.**

***Index Terms*—Adaptive control, backstepping control, induction servomotor, recurrent neural network (RNN).**

I. Introduction

THE neural-network (NN)-based control technique has represented an alternative method for solving problems in control engineering [1]–[4]. It is well known that the neural network (NN) is capable of approximating linear or nonlinear mapping through learning. By adequately choosing network structures, training methods, and sufficient input data, the NN controllers have been developed to compensate for the effects of nonlinearities and system uncertainties, so that the stability, error convergence, and robustness of the control system can be improved. However, the NNs presented in [1]–[4] are the feedforward NNs, they belong to static mapping networks. On the other hand, the recurrent NN (RNN) has capabilities superior to the feedforward NN, such as dynamic response and the information-storing ability [5]–[9]. Since the RNN has a feedback loop, it captures the dynamic response of a system with external feedback through delays. Thus, the RNN is a dynamic mapping network and demonstrates good control performance in the presence of uncertainties, which are usually caused by unpredictable plant-parameter variations, external-force disturbance, and unmodeled nonlinear dynamics in the practical application of dynamic systems.

In the past decade, interest in adaptive control has been increasing and many significant developments have been achieved. In order to guarantee global stability, some restrictions had been made, such as matching condition and extended condition [10]. In an attempt to overcome these restrictions, research on adaptive-backstepping control has increased [10]–[13]. Adaptive backstepping is a systematic and recursive design methodology for nonlinear feedback control and offers a choice for accommodating unmodeled nonlinear effects and parameter uncertainty.

Induction servomotors are used in many automatic systems, including drives for printers, tap recorders, robot manipulators, etc. Recently, decoupled control approaches, such as field-oriented control and nonlinear-state feedback techniques, has been used in the design of induction-servomotor drives for high-performance applications [14], [15]. Using decoupled-control approaches, the dynamic behavior of the induction servomotor is rather similar to that of a separately excited dc motor. However, in the field-oriented method, the decoupled relationship is obtained through the proper selection of state coordinates, under the hypothesis that the rotor flux is kept constant. Therefore, the rotor speed is only asymptotically decoupled from rotor flux, and the speed is linearly related to torque current only after the rotor flux reaches steady-state values. Furthermore, in practical applications, the control performance of the induction servomotor is still influenced by the uncertainties of the plant, such as mechanical-parameter uncertainties, external-load disturbance, and unmodeled dynamics. To deal with these uncertainties, many intelligent techniques have been adopted [13], [16]–[18]. In [13], an adaptive-backstepping control system using a hidden-layer RNN has been proposed, in which the gradient-descent method is used to derive the NN parameter-training algorithms. However, the gradient-descent method cannot guarantee the global convergence of these parameters.

The motivation of this study is to design an RNN-based adaptive-backstepping control (RNABC) system for the

Manuscript received October 8, 2002; revised August 8, 2005. Abstract published on the Internet September 26, 2005. This paper was supported by the National Science Council of the Republic of China under Grant NSC 90-2213-E-155-016.

C.-M. Lin is with the Department of Electrical Engineering, Yuan-Ze University, Tao-Yuan 320, Taiwan, R.O.C. (e-mail: cml@saturn.yzu.edu.tw).

C.-F. Hsu is with the Department of Electrical and Control Engineering, National Chiao-Tung University, Hsinchu 300, Taiwan, R.O.C. (e-mail: fei@cn.nctu.edu.tw).

Digital Object Identifier 10.1109/TIE.2005.858704

position control of the induction servomotor in relation to system-parameter variations. The RNABC system is comprised of a backstepping controller and a robust controller. The backstepping controller containing an RNN uncertainty observer is designed based on the backstepping-control technique, and the robust controller is designed to dispel the effect of approximation error introduced by the uncertainty observer. In this design, an output-feedback RNN is used as the uncertainty observer, which is superior to the hidden-layer RNN presented in [13] in terms of dynamic learning capability [19]. For parameter tuning, the Taylor linearization technique is used in this paper, so that all the parameters of the RNABC system can be tuned at the same time. The adaptive laws of the RNABC system are derived in the sense of the Lyapunov function, so that the stability of the system can be guaranteed. A comparison between IP control and the proposed RNABC is presented. Finally, the simulation and experimental results of the induction-servomotor control are provided to verify the effectiveness of the proposed RNABC scheme with regard to plant variations and input-command frequency variation.

II. Indirect Field-Oriented Induction Servomotor

With the implementation of field-oriented control, the mechanical equation of an induction-servomotor drive can be simplified as [17]

$$J\ddot{\theta}(t) + B\dot{\theta}(t) + T_l = T_e \tag{1}$$

where J is the moment of inertia, B is the damping coefficient, θ is the position, T_l represents the external load disturbance, and T_e denotes the electric torque defined as

$$T_e = K_t i_{qs}^* \tag{2}$$

$$K_t = \left(\frac{3n_p}{2}\right)\left(\frac{L_m^2}{L_r}\right) i_{ds}^* \tag{3}$$

where K_t is the torque constant, i_{qs}^* is the torque-current command, i_{ds}^* is the flux-current command, which will be restrained to $2A$ at the operational points, n_p is the number of pole pairs, L_m is the magnetizing inductance per phase, and L_r is the rotor inductance per phase. Then, the induction-servomotor drive system can be represented in the following form:

$$\begin{aligned}\ddot{\theta}(t) &= -\frac{B}{J}\dot{\theta}(t) + \frac{K_t}{J} i_{qs}^*(t) - \frac{1}{J}T_l \\ &\equiv A_p\dot{\theta}(t) + B_p u(t) + D_p T_l\end{aligned} \tag{4}$$

where $A_p = -B/J$, $B_p = K_t/J > 0$, $D_p = -1/J$, and $u(t) = i_{qs}^*(t)$ is the control effort. Assume that the parameters of the system are well known and the external load disturbance is absent, the nominal model of the induction-servomotor system can be presented as

$$\ddot{\theta}(t) = A_n\dot{\theta}(t) + B_n u(t) \tag{5}$$

where $A_n = -\overline{B}/\overline{J}$ and $B_n = \overline{K}_t/\overline{J}$ are the nominal values of A_p and B_p, and the "$-$" symbol represents the system parameter in the nominal condition. If uncertainties occur, i.e., the parameters of the system deviate from the nominal value or an external load disturbance is added into the system, the controlled system can be modified as

$$\begin{aligned}\ddot{\theta}(t) &= (A_n + \Delta A)\dot{\theta}(t) + (B_n + \Delta B)u(t) + D_p T_l \\ &\equiv A_n\dot{\theta}(t) + B_n u(t) + d(t)\end{aligned} \tag{6}$$

where ΔA and ΔB denote the uncertainties; and $d(t)$ is called the lumped uncertainty defined as $d(t) = \Delta A\dot{\theta}(t) + \Delta B u(t) + D_p T_l$.

III. Recurrent-Neural-Network-Based Adaptive-Backstepping Control System

Since the lumped uncertainty $d(t)$ is time varying and is unknown in practical applications, an RNN is introduced to estimate this uncertainty in the following sections. Then, an RNABC system shown in Fig. 1 is proposed for the induction-servomotor control. The RNABC system is comprised of a backstepping controller with the RNN uncertainty observer and a robust controller.

A. RNN Observer

A three-layer RNN, which is shown in Fig. 2 and is comprised of an input layer, a hidden layer, and an output layer, is utilized to estimate at real time the lumped uncertainty and its structure. The RNN maps according to

$$y(N) = \sum_{k=1}^{n} v_k \Phi_k\left(|x_i(N) w_i y(N-1) - s_{ik}|, \delta_{ik}\right) \tag{7}$$

where x_i, $i = 1, 2, \cdots, m$, and y contain the input variables and the output variable of the RNN, respectively, N is the number of iterations, v_k represents the connective weights between the hidden layer and the output layer, Φ_k represents the firing weight of the kth neuron in the hidden layer, s_{ik} and δ_{ik} are the center and width of the radial basis function, respectively, and w_i is the recurrent weight for the unit in the output layer. The firing weight can be represented as

$$\text{net}_k(N) = \sum_{i=1}^{m} \frac{\left[x_i(N) w_i y(N-1) - s_{ik}\right]^2}{\delta_{ik}^2} \tag{8}$$

and

$$\Phi_k(N) = \mathrm{e}^{-\text{net}_k(N)}. \tag{9}$$

For ease of notation, we define vectors $\boldsymbol{\delta}$, $\mathbf{s}$, $\mathbf{x}$, and $\mathbf{w}$ by collecting all the parameters of the hidden layer in RNN as

$$\boldsymbol{\delta} = [\delta_{11} \cdots \delta_{m1} \delta_{12} \cdots \delta_{m2} \cdots\cdots \delta_{1n} \cdots \delta_{mn}]^{\mathrm{T}} \tag{10}$$

$$\mathbf{s} = [s_{11} \cdots s_{m1} s_{12} \cdots s_{m2} \cdots\cdots s_{1n} \cdots s_{mn}]^{\mathrm{T}} \tag{11}$$

$$\mathbf{x} = [x_1 \cdots x_m]^{\mathrm{T}} \tag{12}$$

$$\mathbf{w} = [w_1 \cdots w_m]^{\mathrm{T}}. \tag{13}$$

Then, the output of the RNN can be represented in vector form

$$y(\mathbf{x}, \boldsymbol{\delta}, \mathbf{s}, \mathbf{w}, \mathbf{v}) = \mathbf{v}^{\mathrm{T}} \boldsymbol{\Phi}(\mathbf{x}, \boldsymbol{\delta}, \mathbf{s}, \mathbf{w}) \tag{14}$$

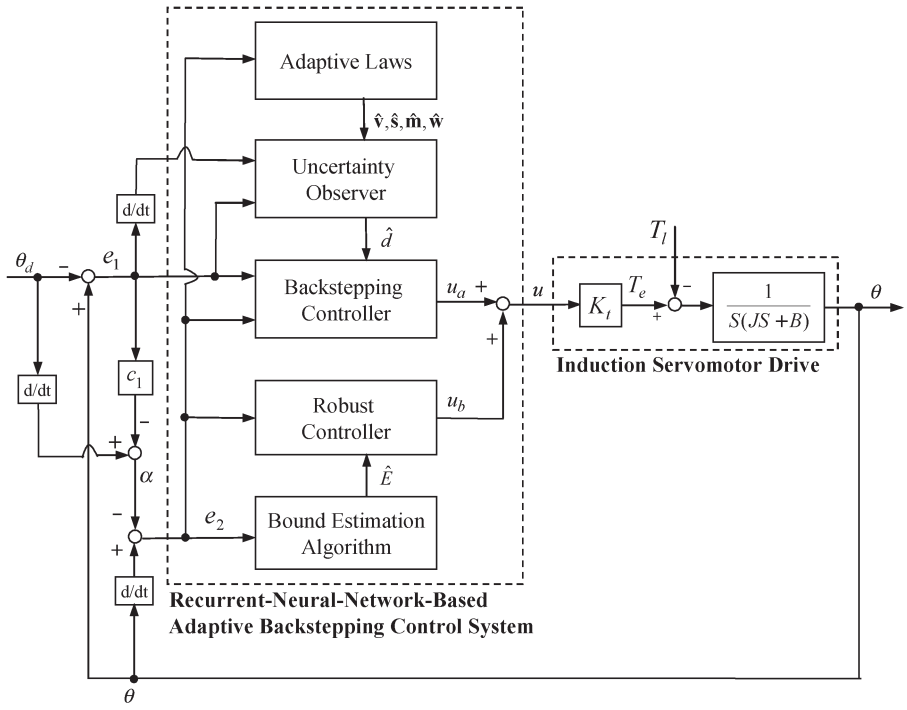

Fig. 1. Block diagram of the RNABC induction-servomotor system.

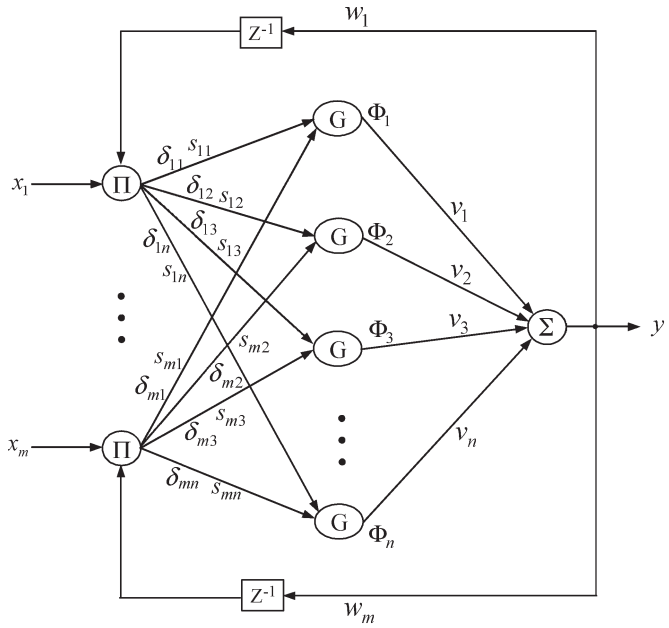

Fig. 2. Structure of an RNN.

where $\mathbf{v} = [v_1\ v_2\ \cdots\ v_n]^{\mathrm{T}}$ and $\mathbf{\Phi} = [\Phi_1\ \Phi_2\ \cdots\ \Phi_n]^{\mathrm{T}}$. It has been proven that there exists an RNN of (14) such that it can uniformly approximate a nonlinear, even time-varying, function [20]. The introduced RNN takes the recurrent connection from the output feedback to the input. This RNN is superior to the hidden-layer RNN presented in [13] and to the dynamic learning capability presented in [19], in which the recurrent connection was taken inside the hidden layer.

In this study, an RNN uncertainty observer is designed to estimate the system uncertainty. The output of the RNN uncertainty observer is the estimated lumped uncertainty $\hat{d}$. By the universal approximation theorem, there exists an optimal RNN approximation d^* such that [20]

$$d = d^* + \Delta = \mathbf{v}^{*\mathrm{T}}\mathbf{\Phi}^* + \Delta \tag{15}$$

where Δ denotes an approximation error, and $\mathbf{v}^*$ and $\mathbf{\Phi}^*$ are the optimal-parameter vectors of $\mathbf{v}$ and $\mathbf{\Phi}$, respectively. The RNN uncertainty observer is defined as

$$\hat{d} = \hat{\mathbf{v}}^{\mathrm{T}}\hat{\mathbf{\Phi}} \tag{16}$$

where $\hat{\mathbf{v}}$ and $\hat{\mathbf{\Phi}}$ are the estimated vectors of $\mathbf{v}^*$ and $\mathbf{\Phi}^*$, respectively. Define the estimated error $\tilde{d}$ as

$$\tilde{d} = d - \hat{d} = d^* - \hat{d} + \Delta = \tilde{\mathbf{v}}^{\mathrm{T}}\hat{\mathbf{\Phi}} + \hat{\mathbf{v}}^{\mathrm{T}}\tilde{\mathbf{\Phi}} + \tilde{\mathbf{v}}^{\mathrm{T}}\tilde{\mathbf{\Phi}} + \Delta \tag{17}$$

where $\tilde{\mathbf{v}} \equiv \mathbf{v}^* - \hat{\mathbf{v}}$ and $\tilde{\mathbf{\Phi}} \equiv \mathbf{\Phi}^* - \hat{\mathbf{\Phi}}$. In the following, the adaptive laws will be derived to online tune the center, width, and recurrent weights of the RNN observer. For achieving this goal, the Taylor-expansion linearization technique is employed to transform the nonlinear radial basis function into a partially linear form

$$\begin{aligned}\tilde{\mathbf{\Phi}} &= \begin{bmatrix} \tilde{\mathbf{\Phi}}_1 \\ \tilde{\mathbf{\Phi}}_2 \\ \vdots \\ \tilde{\mathbf{\Phi}}_n \end{bmatrix} \\ &= \begin{bmatrix} \frac{\partial \mathbf{\Phi}_1}{\partial \boldsymbol{\delta}} \\ \frac{\partial \mathbf{\Phi}_2}{\partial \boldsymbol{\delta}} \\ \vdots \\ \frac{\partial \mathbf{\Phi}_n}{\partial \boldsymbol{\delta}} \end{bmatrix} \Big|_{\boldsymbol{\delta}=\hat{\boldsymbol{\delta}}} \tilde{\boldsymbol{\delta}} + \begin{bmatrix} \frac{\partial \mathbf{\Phi}_1}{\partial \mathbf{s}} \\ \frac{\partial \mathbf{\Phi}_2}{\partial \mathbf{s}} \\ \vdots \\ \frac{\partial \mathbf{\Phi}_n}{\partial \mathbf{s}} \end{bmatrix} \Big|_{\mathbf{s}=\hat{\mathbf{s}}} \tilde{\mathbf{s}} + \begin{bmatrix} \frac{\partial \mathbf{\Phi}_1}{\partial \mathbf{w}} \\ \frac{\partial \mathbf{\Phi}_2}{\partial \mathbf{w}} \\ \vdots \\ \frac{\partial \mathbf{\Phi}_n}{\partial \mathbf{w}} \end{bmatrix} \Big|_{\mathbf{w}=\hat{\mathbf{w}}} \tilde{\mathbf{w}} + \mathbf{h} \end{aligned} \tag{18}$$

or

$$\tilde{\mathbf{\Phi}} = \mathbf{A}^{\mathrm{T}}\tilde{\boldsymbol{\delta}} + \mathbf{B}^{\mathrm{T}}\tilde{\mathbf{s}} + \mathbf{C}^{\mathrm{T}}\tilde{\mathbf{w}} + \mathbf{h} \tag{19}$$

where $\mathbf{A} = [(\partial\Phi_1/\partial\boldsymbol{\delta})\cdots(\partial\Phi_n/\partial\boldsymbol{\delta})]|_{\boldsymbol{\delta}=\hat{\boldsymbol{\delta}}}$; $\mathbf{B} = [(\partial\Phi_1/\partial\mathbf{s}) \cdots (\partial\Phi_n/\partial\mathbf{s})]|_{\mathbf{s}=\hat{\mathbf{s}}}$; $\mathbf{C} = [(\partial\Phi_1/\partial\mathbf{w}) \cdots (\partial\Phi_n/\partial\mathbf{w})]|_{\mathbf{w}=\hat{\mathbf{w}}}$; $\mathbf{h}$ is a vector of higher order terms; $\tilde{\boldsymbol{\delta}} \equiv \boldsymbol{\delta}^* - \hat{\boldsymbol{\delta}}$; $\tilde{\mathbf{s}} \equiv \mathbf{s}^* - \hat{\mathbf{s}}$; $\tilde{\mathbf{w}} \equiv \mathbf{w}^* - \hat{\mathbf{w}}$; $\boldsymbol{\delta}^*$, $\mathbf{s}^*$, and $\mathbf{w}^*$ are the optimal parameter vectors of $\boldsymbol{\delta}$, $\mathbf{s}$, and $\mathbf{w}$, respectively; $\hat{\boldsymbol{\delta}}$, $\hat{\mathbf{s}}$, and $\hat{\mathbf{w}}$ are the estimated parameter vectors of $\boldsymbol{\delta}^*$, $\mathbf{s}^*$, and $\mathbf{w}^*$, respectively, and $\partial\Phi_k/\partial\boldsymbol{\delta}$, $\partial\Phi_k/\partial\mathbf{s}$, and $\partial\Phi_k/\partial\mathbf{w}$ are defined as

$$\left[\frac{\partial\Phi_k}{\partial\boldsymbol{\delta}}\right]^{\mathrm{T}} = \left[\underbrace{0\cdots0}_{(k-1)\times m} \ \frac{\partial\Phi_k}{\partial\delta_{1k}} \ \cdots \ \frac{\partial\Phi_k}{\partial\delta_{mk}} \ \underbrace{0\cdots0}_{(n-k)\times m}\right] \tag{20}$$

$$\left[\frac{\partial\Phi_k}{\partial\mathbf{s}}\right]^{\mathrm{T}} = \left[\underbrace{0\cdots0}_{(k-1)\times m} \ \frac{\partial\Phi_k}{\partial s_{1k}} \ \cdots \ \frac{\partial\Phi_k}{\partial s_{mk}} \ \underbrace{0\cdots0}_{(n-k)\times m}\right] \tag{21}$$

$$\left[\frac{\partial\Phi_k}{\partial\mathbf{w}}\right]^{\mathrm{T}} = \left[\underbrace{0\cdots0}_{(k-1)} \ \frac{\partial\Phi_k}{\partial w_k} \ \underbrace{0\cdots0}_{(n-k)}\right]. \tag{22}$$

Substituting (19) into (17), it can be obtained that

$$\begin{aligned}\tilde{d} &= \tilde{\mathbf{v}}^{\mathrm{T}}\hat{\mathbf{\Phi}} + \hat{\mathbf{v}}^{\mathrm{T}}(\mathbf{A}^{\mathrm{T}}\tilde{\boldsymbol{\delta}} + \mathbf{B}^{\mathrm{T}}\tilde{\mathbf{s}} + \mathbf{C}^{\mathrm{T}}\tilde{\mathbf{w}} + \mathbf{h}) + \tilde{\mathbf{v}}^{\mathrm{T}}\tilde{\mathbf{\Phi}} + \Delta \\ &= \tilde{\mathbf{v}}^{\mathrm{T}}\hat{\mathbf{\Phi}} + \hat{\mathbf{v}}^{\mathrm{T}}\mathbf{A}^{\mathrm{T}}\tilde{\boldsymbol{\delta}} + \hat{\mathbf{v}}^{\mathrm{T}}\mathbf{B}^{\mathrm{T}}\tilde{\mathbf{s}} \\ &\quad + \hat{\mathbf{v}}^{\mathrm{T}}\mathbf{C}^{\mathrm{T}}\tilde{\mathbf{w}} + \hat{\mathbf{v}}^{\mathrm{T}}\mathbf{h} + \tilde{\mathbf{v}}^{\mathrm{T}}\tilde{\mathbf{\Phi}} + \Delta \\ &= \tilde{\mathbf{v}}^{\mathrm{T}}\hat{\mathbf{\Phi}} + \tilde{\boldsymbol{\delta}}^{\mathrm{T}}\mathbf{A}\hat{\mathbf{v}} + \tilde{\mathbf{s}}^{\mathrm{T}}\mathbf{B}\hat{\mathbf{v}} + \tilde{\mathbf{w}}^{\mathrm{T}}\mathbf{C}\hat{\mathbf{v}} + \varepsilon\end{aligned} \tag{23}$$

where $\hat{\mathbf{v}}^{\mathrm{T}}\mathbf{A}^{\mathrm{T}}\tilde{\boldsymbol{\delta}} = \tilde{\boldsymbol{\delta}}^{\mathrm{T}}\mathbf{A}\hat{\mathbf{v}}$, $\hat{\mathbf{v}}^{\mathrm{T}}\mathbf{B}^{\mathrm{T}}\tilde{\mathbf{s}} = \tilde{\mathbf{s}}^{\mathrm{T}}\mathbf{B}\hat{\mathbf{v}}$, and $\hat{\mathbf{v}}^{\mathrm{T}}\mathbf{C}^{\mathrm{T}}\tilde{\mathbf{w}} = \tilde{\mathbf{w}}^{\mathrm{T}}\mathbf{C}\hat{\mathbf{v}}$ are used since they are scales; and the approximation-error term $\varepsilon \equiv \hat{\mathbf{v}}^{\mathrm{T}}\mathbf{h} + \tilde{\mathbf{v}}^{\mathrm{T}}\tilde{\mathbf{\Phi}} + \Delta$ is assumed to be bounded by $|\varepsilon| \le E$.

B. Design of RNABC

The idea of backstepping design is to select an appropriate function as a pseudocontrol input and each backstepping stage results in a new pseudocontrol design. When the procedure terminates a feedback design for the true control input, it achieves the original design objective by summing the Lyapunov functions associated with each individual design stage. The RNABC system design for the induction-servomotor position-tracking control is described step by step as follows.

Step 1) Define the tracking error as

$$e_1 = \theta - \theta_d \tag{24}$$

and its derivative as

$$\dot{e}_1 = \dot{\theta} - \dot{\theta}_d \tag{25}$$

where θ_d is the input command. The $\dot{\theta}$ can be viewed as a virtual control in the equation. Define the following stabilizing function

$$\alpha = -c_1 e_1 + \dot{\theta}_d \tag{26}$$

where c_1 is a positive constant.

Step 2) Define $e_2 = \dot{\theta} - \alpha$, then the derivative of e_2 is expressed as

$$\dot{e}_2 = \ddot{\theta} - \dot{\alpha} = \ddot{\theta} - (-c_1\dot{e}_1 + \ddot{\theta}_d) = \ddot{\theta} - \ddot{\theta}_d + c_1\dot{e}_1. \tag{27}$$

It also shows that

$$\dot{e}_1 = e_2 - c_1 e_1. \tag{28}$$

Step 3) The control law is proposed in the following equation:

$$u(t) = u_a(t) + u_b(t) \tag{29}$$

with

$$\begin{aligned}u_a(t) = B_n^{-1}\Big[&-c_2 e_2 - e_1 - A_n\dot{\theta}(t) \\ &-\hat{d} - c_1\dot{e}_1 + \ddot{\theta}_d(t)\Big]\end{aligned} \tag{30}$$

$$u_b(t) = -B_n^{-1}\hat{E}\,\mathrm{sgn}(e_2) \tag{31}$$

where c_2 is also a positive constant. In the backstepping controller u_a, the uncertainty $\hat{d}$ is estimated by the RNN in (16); and in the robust controller u_b, $\hat{E}$ is an estimated value of the approximation-error bound. Applying the control law in (29) to the system in (6), it is obtained that

$$\ddot{\theta}(t) \equiv A_n\dot{\theta}(t) + B_n[u_a(t) + u_b(t)] + d(t). \tag{32}$$

Substituting (30) and (31) into (32) and from (27), it is obtained that

$$\begin{aligned}&\ddot{\theta} - \ddot{\theta}_d + c_1\dot{e}_1 \\ &\quad = d - \hat{d} - c_2 e_2 - e_1 - \hat{E}\,\mathrm{sgn}(e_2) \\ &\quad = \dot{e}_2.\end{aligned} \tag{33}$$

Substituting (23) into (33), yields

$$\begin{aligned}\dot{e}_2 = \tilde{\mathbf{v}}^{\mathrm{T}}\hat{\mathbf{\Phi}} + \tilde{\boldsymbol{\delta}}^{\mathrm{T}}\mathbf{A}\hat{\mathbf{v}} + \tilde{\mathbf{s}}^{\mathrm{T}}\mathbf{B}\hat{\mathbf{v}} + \tilde{\mathbf{w}}^{\mathrm{T}}\mathbf{C}\hat{\mathbf{v}} \\ + \varepsilon - c_2 e_2 - e_1 - \hat{E}\,\mathrm{sgn}(e_2).\end{aligned} \tag{34}$$

Step 4) Define the Lyapunov function as

$$\begin{aligned}&V\left(e_1, e_2, \tilde{E}(t), \tilde{\mathbf{v}}, \tilde{\boldsymbol{\delta}}, \tilde{\mathbf{s}}, \tilde{\mathbf{w}}\right) \\ &\quad = \frac{1}{2}e_1^2 + \frac{1}{2}e_2^2 + \frac{1}{2\eta_1}\tilde{E}^2(t) + \frac{1}{2\eta_2}\tilde{\mathbf{v}}^{\mathrm{T}}\tilde{\mathbf{v}} \\ &\qquad + \frac{1}{2\eta_3}\tilde{\boldsymbol{\delta}}^{\mathrm{T}}\tilde{\boldsymbol{\delta}} + \frac{1}{2\eta_4}\tilde{\mathbf{s}}^{\mathrm{T}}\tilde{\mathbf{s}} + \frac{1}{2\eta_5}\tilde{\mathbf{w}}^{\mathrm{T}}\tilde{\mathbf{w}}\end{aligned} \tag{35}$$

where $\tilde{E}(t) = E - \hat{E}(t)$; and η_1, η_2, η_3, η_4, and η_5 are positive constants.

Differentiating (35) with respect to time and using (28) and (34), it is obtained that

$$\begin{aligned}\dot{V} &= e_1\dot{e}_1 + e_2\dot{e}_2 + \frac{\tilde{E}\dot{\tilde{E}}}{\eta_1} + \frac{\tilde{\mathbf{v}}^{\mathrm{T}}\dot{\tilde{\mathbf{v}}}}{\eta_2} + \frac{\tilde{\boldsymbol{\delta}}^{\mathrm{T}}\dot{\tilde{\boldsymbol{\delta}}}}{\eta_3} + \frac{\tilde{\mathbf{s}}^{\mathrm{T}}\dot{\tilde{\mathbf{s}}}}{\eta_4} + \frac{\tilde{\mathbf{w}}^{\mathrm{T}}\dot{\tilde{\mathbf{w}}}}{\eta_5} \\ &= e_1(e_2 - c_1e_1) + e_2\left[\tilde{\mathbf{v}}^{\mathrm{T}}\hat{\boldsymbol{\Phi}} + \tilde{\boldsymbol{\delta}}^{\mathrm{T}}\mathbf{A}\hat{\mathbf{v}} + \tilde{\mathbf{s}}^{\mathrm{T}}\mathbf{B}\hat{\mathbf{v}} + \tilde{\mathbf{w}}^{\mathrm{T}}\mathbf{C}\hat{\mathbf{v}}\right. \\ &\qquad \left. + \varepsilon - c_2e_2 - e_1 - \hat{E}\,\mathrm{sgn}(e_2)\right] \\ &\quad + \frac{\tilde{E}\dot{\tilde{E}}}{\eta_1} + \frac{\tilde{\mathbf{v}}^{\mathrm{T}}\dot{\tilde{\mathbf{v}}}}{\eta_2} + \frac{\tilde{\boldsymbol{\delta}}^{\mathrm{T}}\dot{\tilde{\boldsymbol{\delta}}}}{\eta_3} + \frac{\tilde{\mathbf{s}}^{\mathrm{T}}\dot{\tilde{\mathbf{s}}}}{\eta_4} + \frac{\tilde{\mathbf{w}}^{\mathrm{T}}\dot{\tilde{\mathbf{w}}}}{\eta_5} \\ &= -c_1e_1^2 - c_2e_2^2 + \tilde{\mathbf{v}}^{\mathrm{T}}\left(e_2\hat{\boldsymbol{\Phi}} + \frac{\dot{\tilde{\mathbf{v}}}}{\eta_2}\right) \\ &\quad + \tilde{\boldsymbol{\delta}}^{\mathrm{T}}\left(e_2\mathbf{A}\hat{\mathbf{v}} + \frac{\dot{\tilde{\boldsymbol{\delta}}}}{\eta_3}\right) + \tilde{\mathbf{s}}^{\mathrm{T}}\left(e_2\mathbf{B}\hat{\mathbf{v}} + \frac{\dot{\tilde{\mathbf{s}}}}{\eta_4}\right) \\ &\quad + \tilde{\mathbf{w}}^{\mathrm{T}}\left(e_2\mathbf{C}\hat{\mathbf{v}} + \frac{\dot{\tilde{\mathbf{w}}}}{\eta_5}\right) + \varepsilon e_2 - \hat{E}|e_2| + \frac{\tilde{E}\dot{\tilde{E}}}{\eta_1}. \end{aligned} \tag{36}$$

If the adaptive laws for the RNN observer and the approximation-error bound are chosen as

$$\dot{\hat{E}}(t) = -\dot{\tilde{E}}(t) = \eta_1|e_2| \tag{37}$$

$$\dot{\hat{\mathbf{v}}} = -\dot{\tilde{\mathbf{v}}} = \eta_2 e_2\hat{\boldsymbol{\Phi}} \tag{38}$$

$$\dot{\hat{\boldsymbol{\delta}}} = -\dot{\tilde{\boldsymbol{\delta}}} = \eta_3 e_2\mathbf{A}\hat{\mathbf{v}} \tag{39}$$

$$\dot{\hat{\mathbf{s}}} = -\dot{\tilde{\mathbf{s}}} = \eta_4 e_2\mathbf{B}\hat{\mathbf{v}} \tag{40}$$

$$\dot{\hat{\mathbf{w}}} = -\dot{\tilde{\mathbf{w}}} = \eta_5 e_2\mathbf{C}\hat{\mathbf{v}} \tag{41}$$

then (36) becomes

$$\begin{aligned}&\dot{V}\left(e_1, e_2, \tilde{E}(t), \tilde{\mathbf{v}}, \tilde{\boldsymbol{\delta}}, \tilde{\mathbf{s}}, \tilde{\mathbf{w}}\right) \\ &\quad = -c_1e_1^2 - c_2e_2^2 + \varepsilon e_2 - E|e_2| \\ &\quad \le -c_1e_1^2 - c_2e_2^2 - (E - |\varepsilon|)\,|e_2| \le 0. \end{aligned} \tag{42}$$

In summary, the RNABC system is designed as in (29), which is comprised of a backstepping controller in (30) and a robust controller in (31). In the backstepping controller, the lumped uncertainty is estimated by an RNN in (16), where the parameters $\hat{\mathbf{v}}$, $\hat{\boldsymbol{\delta}}$, $\hat{\mathbf{s}}$, and $\hat{\mathbf{w}}$ of the RNN observer are adjusted by (38) through (41). In the robust controller, the approximation-error bound is estimated by (37). With this control system, the system stability can be guaranteed.

IV. Simulation and Experimental Results

The curve-fitting technique based on step–position response is applied to find the model of the drive system in the nominal condition ($T_l = 0$ N · m without parameter variations). The results are

$$\begin{aligned}\overline{K}_t &= 0.6851\ \mathrm{N\cdot m/A} \\ \overline{J} &= 0.25 \times 10^{-3}\ \mathrm{N\cdot m\cdot s^2} \\ \overline{B} &= 19.84 \times 10^{-3}\ \mathrm{N\cdot m\cdot s/rad}. \end{aligned} \tag{43}$$

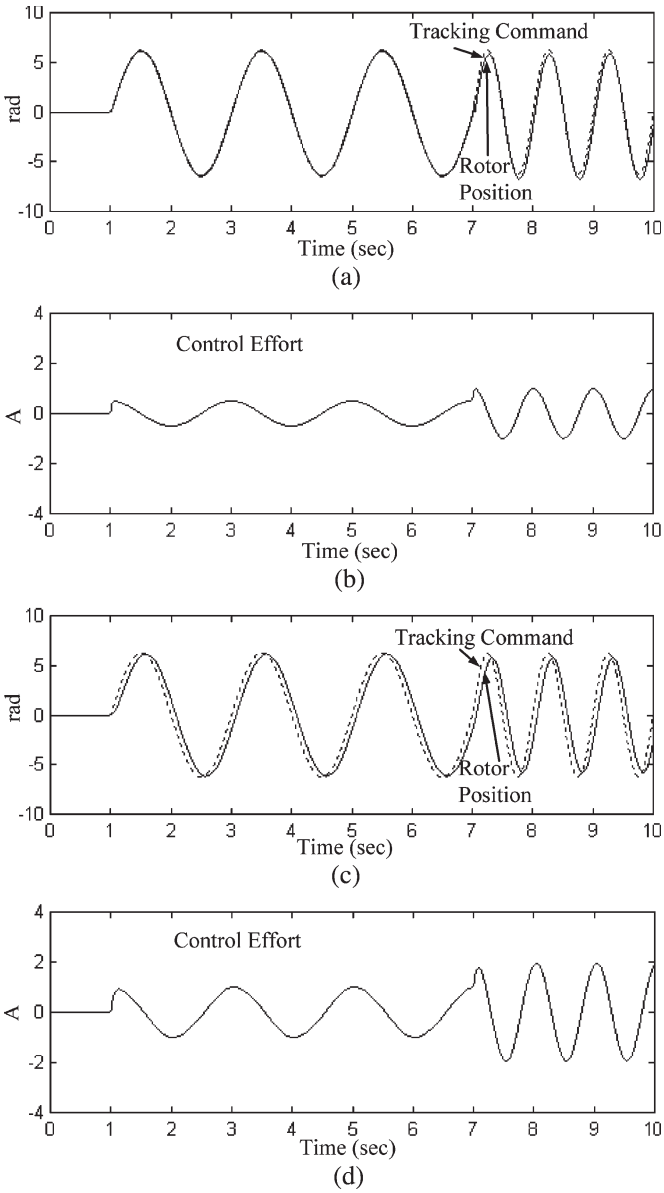

Fig. 3. Simulation results of the IP-control induction-servomotor system due to a sinusoidal command.

To investigate the effectiveness of the proposed RNABC system, two simulation cases including parameter variations are considered as

$$\text{Case 1}: J = \overline{J}, B = \overline{B} \tag{44}$$

$$\text{Case 2}: J = 2 \times \overline{J}, B = 2 \times \overline{B}. \tag{45}$$

In (28) and (30), c_1 and c_2 will influence the convergent speed of e_1 and e_2, respectively; however, they also influence the control gain of u_a. In (38) through (41), the parameters η_2, η_3, η_4, and η_5 are the leaning rates of the RNN. If η_2, η_3, η_4, and η_5 are chosen to be small, then the parameter convergence of the RNN can be achieved; however, this will result in slow learning speed. On the other hand, if η_2, η_3, η_4, and η_5 are chosen to be large, then the learning speed will be fast; however, the RNN system may become more unstable for the parameter convergence. In (37),

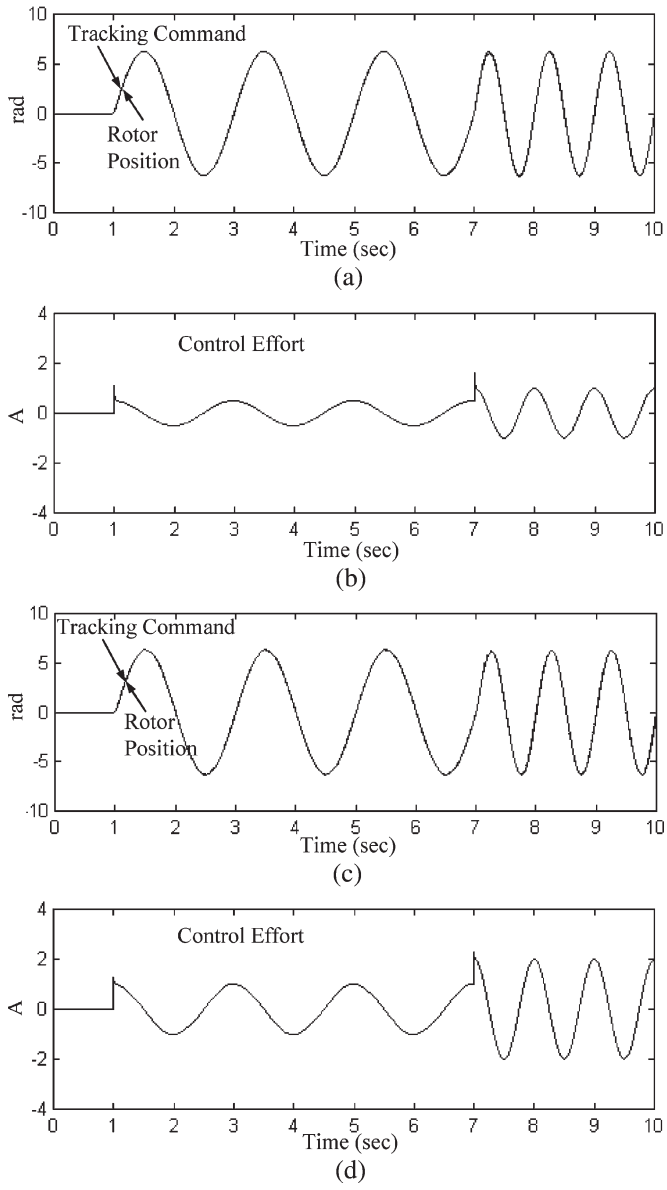

Fig. 4. Simulation results of the RNABC induction-servomotor system due to a sinusoidal command.

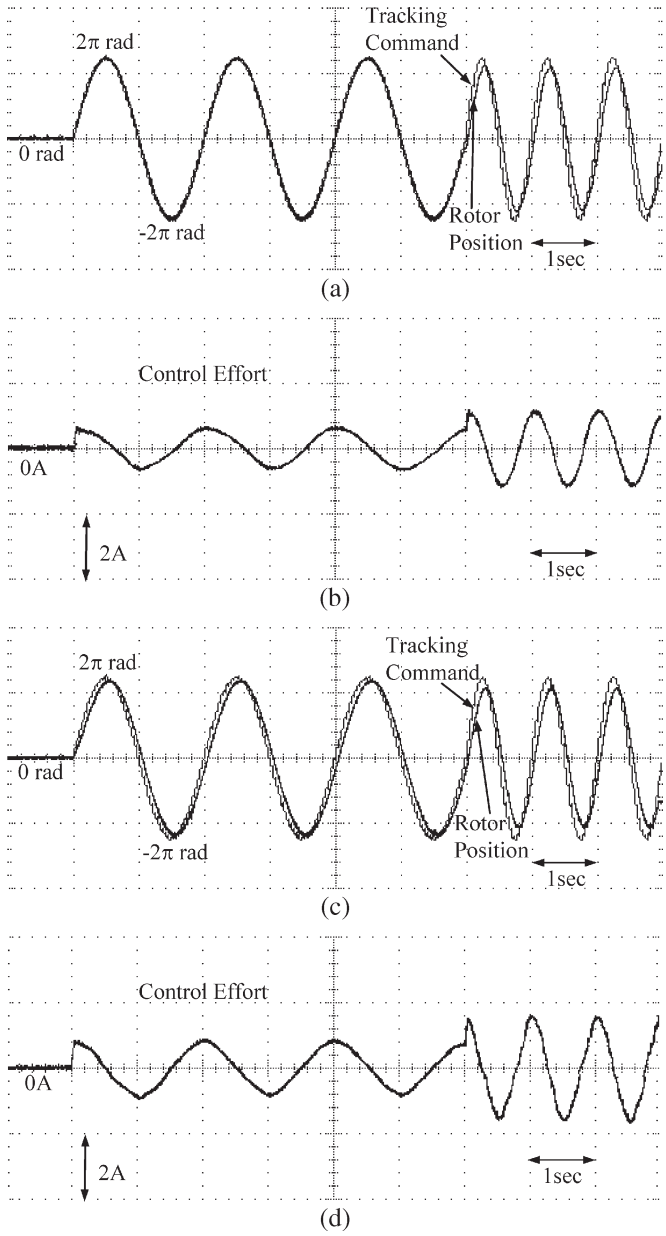

Fig. 5. Experimental results of the IP-control induction-servomotor system due to a sinusoidal command.

the parameter η_1 is the learning rate of the approximation-error bound. Similar to η_2, η_3, η_4, and η_5, the choice of η_1 will influence the convergent speed of the error bound. The parameters in control systems are chosen as $c_1 = 20$, $c_2 = 20$, $\eta_1 = 0.1$, and $\eta_2 = \eta_3 = \eta_4 = \eta_5 = 100$. These parameters are chosen through trials to achieve a favorable control performance.

In the simulations, an IP control system is considered for comparison [17]. The simulation results of an IP induction-servomotor system due to a sinusoidal command are shown in Fig. 3, in which the frequency of the sinusoidal command is doubled at the seventh second. The tracking responses are shown in Fig. 3(a) and (c); and the associated control efforts are shown in Fig. 3(b) and (d) for cases 1 and 2, respectively. From Fig. 3(a), accurate tracking performance can be obtained at the first 7 s; however, degenerate tracking responses are produced when the frequency of the input command is increased at the seventh second. Fig. 3(b) shows that when parameter variation occurs, degenerate tracking responses always result. For comparison, the proposed RNABC scheme is applied for an induction-servomotor control system with the same simulation conditions. The simulation results are shown in Fig. 4. The tracking responses are shown in Fig. 4(a) and (c); and the associated control efforts are shown in Fig. 4(b) and (d) for cases 1 and 2, respectively. The simulation results show that the RNABC can achieve favorable tracking performance even in relation to parameter variations and input-command frequency variation.

Some experimental results are provided to further demonstrate the effectiveness of the proposed control scheme. Two experimental conditions are demonstrated; one is the condition where the rotor inertia is the nominal value (condition 1), and the other is the condition 2, which increases the rotor

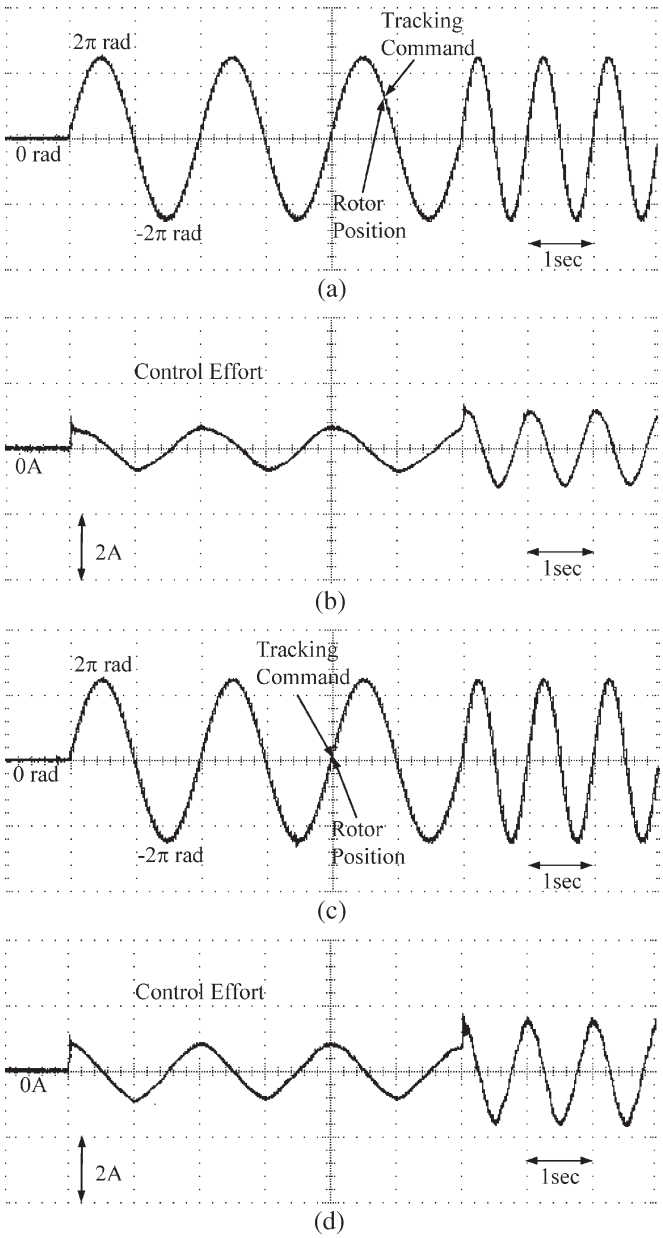

Fig. 6. Experimental results of the RNABC induction-servomotor system due to a sinusoidal command.

inertia to approximate two times that of the nominal value; and doubles the frequency of the sinusoidal command at the seventh second. The experimental results of IP control and RNABC due to the sinusoidal command are shown in Figs. 5 and 6, respectively. The experimental results confirm the results of the simulation, that the proposed RNABC can achieve better control performance than the IP control.

V. Conclusion

This study has successfully demonstrated the application of a recurrent-neural-network (RNN)-based adaptive-backstepping control (RNABC) system, which is comprised of a backstepping controller with an RNN uncertainty observer and a robust controller, to the position control of an induction servomotor. The uncertainty observer uses an RNN to estimate the lumped uncertainty in real time. All the adaptive laws of the RNABC system are derived in the sense of the Lyapunov function, so that the stability of the system can be guaranteed. Moreover, simulation and experimental results were carried out to illustrate the effectiveness of the proposed control system. Finally, a comparison between IP control and the proposed RNABC is presented. The simulation and experimental results show that the proposed RNABC has achieved better control performance than the IP control.

Acknowledgment

The authors are grateful to the reviewers for their valuable comments.

References

[1] M. Zhihong, H. R. Wu, and M. Palaniswami, "An adaptive tracking controller using neural networks for a class of nonlinear systems," *IEEE Trans. Neural Netw.*, vol. 9, no. 5, pp. 947–1031, Sep. 1998.

[2] S. S. Ge, C. C. Hang, and T. Zhang, "Adaptive neural network control of nonlinear systems by state and output feedback," *IEEE Trans. Syst., Man, Cybern. B, Cybern.*, vol. 29, no. 6, pp. 818–828, Dec. 1999.

[3] S. Seshagiri and H. K. Khalil, "Output feedback control of nonlinear systems using RBF neural networks," *IEEE Trans. Neural Netw.*, vol. 11, no. 1, pp. 69–79, Jan. 2000.

[4] C. M. Lin and C. F. Hsu, "Neural network hybrid control for antilock braking systems," *IEEE Trans. Neural Netw.*, vol. 14, no. 2, pp. 351–359, Mar. 2003.

[5] C. C. Ku and K. Y. Lee, "Diagonal recurrent neural networks for dynamic systems control," *IEEE Trans. Neural Netw.*, vol. 6, no. 1, pp. 144–156, Jan. 1995.

[6] T. W. S. Chow and Y. Fang, "A recurrent neural-network-based real-time learning control strategy applied to nonlinear systems with unknown dynamics," *IEEE Trans. Ind. Electron.*, vol. 45, no. 1, pp. 151–161, Feb. 1998.

[7] C. H. Lee and C. C. Teng, "Identification and control of dynamic systems using recurrent fuzzy neural networks," *IEEE Trans. Fuzzy Syst.*, vol. 8, no. 4, pp. 349–366, Aug. 2000.

[8] C. M. Lin and C. F. Hsu, "Recurrent neural network adaptive control of wing rock motion," *J. Guid. Control Dyn.*, vol. 25, no. 6, pp. 1163–1165, Jun. 2002.

[9] ——, "Supervisory recurrent fuzzy neural network control of wing rock for slender delta wings," *IEEE Trans. Fuzzy Syst.*, vol. 12, no. 5, pp. 733–742, Oct. 2004.

[10] M. Krstic, I. Kanellakopoulos, and P. V. Kokotovic, *Nonlinear and Adaptive Control Design*. New York: Wiley, 1995.

[11] H. J. Shieh and K. K. Shyu, "Nonlinear sliding-mode torque control with adaptive backstepping approach for induction motor drive," *IEEE Trans. Ind. Electron.*, vol. 46, no. 2, pp. 380–389, Apr. 1999.

[12] T. Zhang, S. S. Ge, and C. C. Hang, "Adaptive neural network control for strict-feedback nonlinear systems using backstepping design," *Automatica*, vol. 36, no. 12, pp. 1835–1846, Dec. 2000.

[13] F. J. Lin, R. J. Wai, W. D. Chou, and S. P. Hsu, "Adaptive backstepping control using recurrent neural network for linear induction motor drive," *IEEE Trans. Ind. Electron.*, vol. 49, no. 1, pp. 134–146, Feb. 2002.

[14] C. M. Liaw and F. J. Lin, "Position control with fuzzy adaptation for induction servomotor drive," *Proc. IEE—Electr. Power Appl.*, vol. 142, no. 6, pp. 397–404, Nov. 1995.

[15] C. M. Lin and C. F. Hsu, "Adaptive fuzzy sliding-mode control for induction servomotor systems," *IEEE Trans. Energy Convers.*, vol. 19, no. 2, pp. 362–368, Jun. 2004.

[16] T. C. Huang and M. A. El-Sharkawi, "High performance speed and position tracking of induction motors using multi-layer fuzzy control," *IEEE Trans. Energy Convers.*, vol. 11, no. 2, pp. 353–358, Jun. 1996.

[17] F. J. Lin, R. J. Wai, C. H. Lin, and D. C. Liu, "Decoupled stator-flux-oriented induction motor drive with fuzzy neural network uncertainty observer," *IEEE Trans. Ind. Electron.*, vol. 47, no. 2, pp. 356–367, Apr. 2000.

[18] C. M. Lin and C. F. Hsu, "Neural-network-based adaptive control for induction servomotor drive system," *IEEE Trans. Ind. Electron.*, vol. 49, no. 1, pp. 115–123, Feb. 2002.

[19] C. T. Lin and C. S. G. Lee, *Neural Fuzzy Systems: A Neuro-Fuzzy Synergism to Intelligent Systems*. Englewood Cliffs, NJ: Prentice-Hall, 1996.

[20] L. X. Wang, *Adaptive Fuzzy Systems and Control: Design and Stability Analysis*. Englewood Cliffs, NJ: Prentice-Hall, 1994.

Chih-Min Lin (S'86–M'87–SM'99) received the B.S. and M.S. degrees in control engineering and the Ph.D. degree in electronics engineering from National Chiao Tung University, Taiwan, R.O.C., in 1981, 1983, and 1986, respectively.

From 1986 to 1992, he was with the Chung Shan Institute of Science and Technology as a Deputy Director of system engineering of missile systems. He also served concurrently as an Associate Professor at Chiao Tung University and Chung Yuan University, Taiwan, R.O.C. He joined the faculty of the Department of Electrical Engineering, Yuan-Ze University, Tao-Yuan, Taiwan, R.O.C., in 1993 and is currently a Professor and the Chairman of the Department of Electrical Engineering. From 1997 to 1998, he was the Honor Research Fellow in the University of Auckland, New Zealand. His research interests include fuzzy neural networks (NNs), cerebellar-model articulation control, guidance and flight control, and systems engineering.

Dr. Lin has served as a Committee Member of the Chinese Automatic Control Society and as Deputy Chairman of the IEEE Control Systems Society, Taipei Section.

Chun-Fei Hsu (M'05) received the B.S., M.S., and Ph.D. degrees in electrical engineering from Yuan-Ze University, Tao-Yuan, Taiwan, R.O.C., in 1997, 1999, and 2002, respectively.

After graduation, he joined the Department of Electrical and Control Engineering, National Chiao-Tung University, Hsinchu, Taiwan, R.O.C. From 2002 to 2005, he was conducting postdoctoral research on virtual-reality dynamic simulators and intelligent transportation systems. His research interests include servomotor drives, adaptive control, flight control, and intelligent control using fuzzy-system and neural-network technologies.